JMEPEG (2010) 19:142–149
DOI: 10.1007/s11665-009-9386-x

1059-9495/$19.00

The Nature of the Tensile Fracture in Austempered Ductile Iron with Dual Matrix Microstructure

Volkan Kilicli and Mehmet Erdogan

(Submitted August 3, 2007; in revised form February 3, 2009)

The tensile fracture characteristics of austempered ductile irons with dual matrix structures and different ausferrite volume fractions have been studied for an unalloyed ductile cast iron containing (in wt.%) 3.50 C, 2.63 Si, 0.318 Mn, and 0.047 Mg. Specimens were intercritically austenitized (partially austenitized) in two phase region ($\alpha + \gamma$) at various temperatures for 20 min and then quenched into a salt bath held at austempering temperature of 365 °C for various times and then air cooled to room temperature to obtain various ausferrite volume fractions. Conventionally austempered specimens with fully ausferritic matrix and unalloyed as-cast specimens having fully ferritic structures were also tested for comparison. In dual matrix structures, results showed that the volume fraction of proeutectoid ferrite, new (epitaxial) ferrite, and ausferrite [bainitic ferrite + high-carbon austenite (stabilized or transformed austenite)] can be controlled to influence the strength and ductility. Generally, microvoids nucleation is initiated at the interface between the graphite nodules and the surrounding ferritic structure and at the grain boundary junctions in the fully ferritic microstructure. Debonding of the graphite nodules from the surrounding matrix structure was evident. The continuity of the ausferritic structure along the intercellular boundaries plays an important role in determining the fracture behavior of austempered ductile iron with different ausferrite volume fractions. The different fracture mechanisms correspond to the different levels of ausferrite volume fractions. With increasing continuity of the ausferritic structure, fracture pattern changed from ductile to moderate ductile nature. On the other hand, in the conventionally austempered samples with a fully ausferritic structure, the fracture mode was a mixture of quasi-cleavage and a dimple pattern. Microvoid coalescence was the dominant form of fracture in all structures.

Keywords ausferrite volume fraction, austempered ductile iron, dual matrix structure, tensile fracture

1. Introduction

In the newly developed ductile iron with dual matrix structure (DMS), the structure composed of proeutectoid ferrite and ausferrite, i.e., bainitic ferrite and high-carbon austenite (stabilized or transformed austenite) or martensite (Ref 1-13). In this work, austempered ductile iron (ADI) with DMS was obtained by austempering from intercritical austenitizing temperature (ICAT) or partial austenitizing temperature ranges which corresponds to the ($\alpha + \gamma +$ graphite) region. In this article, this is referred to as the ($\alpha + \gamma$) temperature range.

Austempered ductile iron is a very attractive material for some applications such as automotive suspension where a good combination of high strength and ductility is required. This newly developed ADI with DMS exhibits a similar tensile and proof stress, and hardness to pearlitic grades, and possesses a ductility comparable to ferritic grades (Ref 3).

In literature, very little information is currently available on the mechanical properties of ADI with DMS (Ref 1-3). Recently, the present authors (Ref 13) have shown that the volume fraction of ausferrite, proeutectoid ferrite, and new ferrite (epitaxial ferrite) can be controlled to influence the strength and ductility. ADI with ~47.2% ausferrite volume fraction (AFVF) exhibited an excellent combination of high strength and ductility. The strength and ductility of this material is much higher than the ferritic grades and its strength is comparable to that of the pearlitic grades, but the ductility is nearly four times higher than the pearlitic grades. The material with ~75% AFVF exhibited the best combination of high strength and ductility compared with pearlitic grades but with slightly reduced ductility relative to ferritic grades. This material also satisfies the requirements for strength of quenched and tempered grades but with superior ductility.

Previous studies of the tensile fracture behavior of ADI with DMS have been performed (Ref 1, 5), but those studies did not report the existence of new ferrite in ADI with DMS or data concerning the AFVFs or proeutectoid ferrite volume fractions which were not controlled in those studies. To determine the effect of AFVF and proeutectoid ferrite volume fraction on the fracture behavior, this study was planned to examine the matrix deformation, microvoid formation, and tensile fracture nature of ADI with DMS as a function of different volume fractions of ausferrite, proeutectoid ferrite, and new ferrite.

Volkan Kilicli and **Mehmet Erdogan**, Materials Division, Metallurgy Education Department, Faculty of Technical Education, Gazi University, 06500 Besevler-Ankara, Turkey. Contact e-mails: vkilicli@gazi.edu.tr, mehmeter@gazi.edu.tr.

2. Experimental Procedure

The chemical composition and microstructure of as-cast unalloyed ductile iron used in this study is given in Table 1. The details of casting and experimental procedure are given elsewhere (Ref 12). As-cast material had ferrite + graphite structure (Fig. 1). The as-cast specimens were the starting point for subsequent austempering heat treatment. The specimens were intercritically annealed at the ICAT of 795, 805, 815, and 830 °C for 20 min and then rapidly transferred to a salt bath containing 50% KNO_3 + 50% $NaNO_3$ held at the 365 °C for austempering for various times to produce DMS with different AFVFs. As-cast samples were also heat treated at the conventional austenitizing temperature of 900 °C and then austempered at the same austempering temperature for comparison. Figure 2 provides a summary of heat treatments. Throughout these heat treatments, the temperature of each specimen was monitored by a thermocouple spot welded to the center of one of its faces.

The specimens were coded according to heat treatment temperature and % of the AFVF. For example, in specimen code 815 (47.2 AFVF), 815 stand for the ICAT and (47.2 AFVF) for the % of the AFVF. The proportions of the constituents presented were determined by point counting on etched (Nital and Chromate) metallographic sections. Between 1000 and 2000 points were counted to keep the standard error of the volume fraction of phases below 6%. The nodule count was 195 mm^{-2}.

The relative amounts of the high-carbon austenite and ferrite volume fractions in all heat-treated specimens were measured by x-ray diffractometry following the standard procedure (Ref 14). X-ray diffraction profiles were obtained on a Brucer D8 x-ray diffractometer at 40 kV and 20 mA using monochromated Cu Kα radiation. The samples were scanned in the 2θ range of 40-100° at a scanning speed of 0.05°/min. The integrated areas of both austenite (220) and (311) and ferrite (211) peaks were used for determination of volume fraction of austenite and ferrite. The bainitic ferrite volume fraction was calculated by substituting the sum of the proeutectoid and new ferrite content calculated by point counting from the x-ray analysis result of the total volume percent of the ferrite (Ref 12, 13). The results of phase proportions are listed in Table 2.

Tensile specimens were machined in accordance with ASTM standard E8 M from the heat-treated materials to remove any decarburized layer. Room temperature tensile tests were performed using a DARTEC machine with 60 kN loading capacity at a cross-head speed of 1 mm/min. An extensometer set to a gage length of 10 mm was used for strain measurement. A minimum of five specimens were tested for each heat-treatment condition and average values were calculated.

After fracture, the specimens were sectioned parallel to the tensile loading direction using a spark (electric discharge machining) machine. The sectioned specimens were ground polished and then etched in 2% nital to assess the crack path and final fracture.

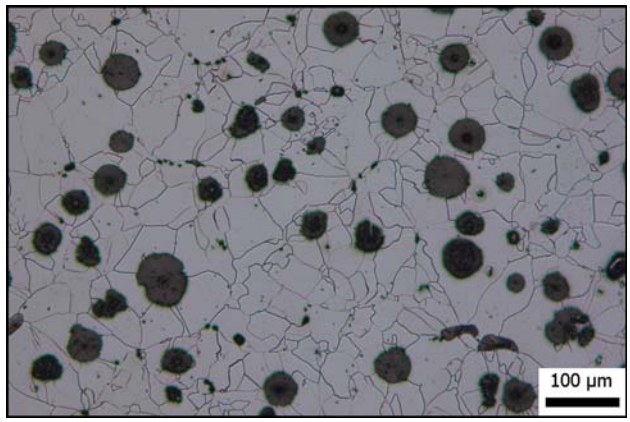

Fig. 1 The starting microstructure of as-cast ductile iron. Etchant: 2% nital

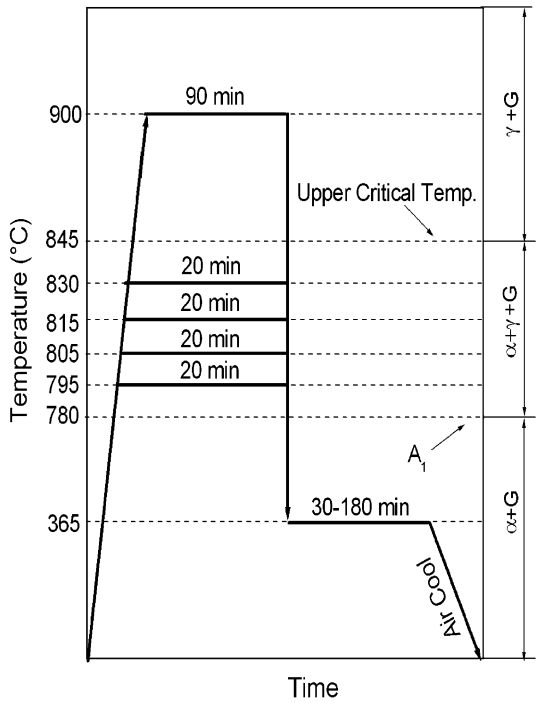

Fig. 2 Summary of heat treatments

Table 1 Chemical composition of unalloyed ductile iron used (wt.%)

C	Si	Mn	P	S	Cr	Mo	Ni	Al	Co
3.50	2.63	0.318	0.019	0.009	0.031	0.0421	0.042	0.003	<0.001
Cu	**Nb**	**Ti**	**V**	**W**	**Pb**	**Sn**	**Mg**	**Sb**	**Fe**
0.055	<0.002	<0.012	<0.001	0.005	<0.0002	0.0058	0.0471	0.0055	Rest

Table 2 Results of metallographic measurement and tensile properties (average values ±3%)

Specimen code	Austem. time, min	High-carbon austenite content, vol.%	Bainitic ferrite content vol.%	Proeutectoid ferrite content, vol.%	Martensite content, vol.%	New ferrite content, vol.%	0.2% Proof stress, MPa	Tensile strength, MPa	Uniform elongation, %	Total elongation, %
A795 (17 AFVF)	30	3.1	5.9	75.3	14.2	1.5	272.9	406.3	20.1	25
	60	5.8	7.6	75.3	6.6	4.7	320.2	456.5	21.3	26
	120	8.1	8.9	75.3	0	7.7	306.3	440.6	22.9	27.5
	180	7.1	7.9	75.3	0	9.7	325.3	460.5	19.4	24.5
A805 (26.4 AFVF)	30	5.8	7.9	52.8	31.8	1.7	288.3	426.4	18.8	23.9
	60	9.9	13.2	52.8	18.3	5.8	329.5	466.7	19.6	24.6
	120	16.4	19.2	52.8	0	11.6	337.8	476.4	20.9	25.9
	180	15.1	20.2	52.8	0	11.9	358.4	490.1	18.8	23.8
A815 (47.2 AFVF)	30	7.9	8.3	38.2	38.2	7.4	345.8	481.2	14.3	18
	60	13.8	14.6	38.2	23.2	10.2	385.1	552	15	19.7
	120	22.5	24.7	38.2	0	14.6	370.2	529.7	18.6	22.7
	180	22.3	24.4	38.2	0	15.1	379.6	532.6	17.4	20
A830 (75 AFVF)(a)	120	27.1	32.9	21.8	0	18.2	518	685.4	13.6	15
C900 (94.5 AFVF)	30	19.3	28.1	···	52.6	···	816	1111.1	3	3
	60	28.5	37.9	···	33.6	···	784	1089.9	10.6	10.6
	120	39.3	55.2	···	5.5	···	778	1085.7	12.1	12.1
	180	37.8	62.2	···	0	···	810	1105.1	10	10
As cast	···	···	···	89.8	···	···	261.5	397	22.7	27.7

(a) A full test programme would have required 30, 60, 120, and 180 min austempering for A830 specimen. In practice, material constraints limited the 30, 60, and 180 min austempering for A830 were missing from the data set

3. Results and Discussion

3.1 Heat Treatments and Microstructures

The changes in the proportions of phases as a function of austempering time are given in Table 2. These results are consistent with the published literature (Ref 3, 4, 8, 15-26).

In this study, austempering from different ICATs produced a DMS consisting of ausferrite and proeutectoid ferrite at the specimens with different AFVFs restricted to eutectic cell boundaries and an isolated or continuous network of ausferritic structure along the eutectic cell boundary formed depending on AFVF (Fig. 3a-d). Eutectic cell boundaries are the potent sites for austenite nucleation. In the conventionally austempered specimen 900 (94.5 AFVF), austempering for 120 min produced a typical ausferritic structure throughout the specimen without martensite (Fig. 3e).

To reveal new (epitaxial) ferrite in ADI with DMS, the chromate etching technique invented by Lawson et al. (Ref 27) was used. Some examples of the microstructures evolved with 120 min austempering time are shown in Fig. 4(a) and (b). Recently, this etching technique was also used to reveal new ferrite in ADI with DMS (Ref 12, 13). In this study, the chromate etching showed that the new ferrite as the bright, white constituent as shown in Fig. 4(a). The new ferrite was absent in conventionally austempered specimen 900 for all austempering times (Fig. 4b). The absence of new ferrite in conventionally austempered sample with higher austenite carbon content was attributed to the sensitive of new ferrite growth rate to carbon concentration in the austenite. For the austenite with higher carbon content, new ferrite growth rate was considerably slower than the austenite with low-carbon content (Ref 12).

3.2 Tensile Fracture

3.2.1 Matrix Deformation and Microvoid Formation. The average values of the 0.2% proof strength, tensile strength, uniform, and total elongation obtained for each heat-treatment conditions investigated are given in Table 2. The optimum combination of strength and ductility in austempered samples are achieved at times corresponding to the austempering for 120 min. For this reason, following discussion will be focused on structure-tensile fracture relationships for samples austempered for 120 min.

Figure 5(a) shows the void formation in necked regions of a fractured as-cast specimen with a fully ferritic matrix. The initial void formation was due to decohesion at the ferrite-graphite interface (Fig. 5a, arrow a). Debonding of the graphite nodules from the surrounding ferrite matrix is evident (Fig. 5a, arrow b). Microvoid nucleations are also initiated at the grain boundary junctions (Fig. 5a, arrow c). The features shown in this figure suggest that ferrite deforms to a great extent before the onset of fracture, which starts by the formation and coalescence of voids. This observation is consistent with the high ductility of this material.

In the specimens with DMS and low AFVFs [795 (17 AFVF) and 805 (26.4 AFVF)], microvoids initiated due to decohesion at the ferrite-graphite interface (Fig. 5b, arrow a) and void nucleation associated with high-carbon austenite resulted either from decohesion at the ferrite-high carbon austenite interface (Fig. 5c, arrow a) or from the separation of adjacent particles (Fig. 5c, arrows b and c) and localized deformation of high-carbon austenite particles at very high strain levels, which was followed by decohesion at the ferrite-graphite and ferrite-high-carbon austenite interfaces. When the strain became severe, a void opened up between two particles.

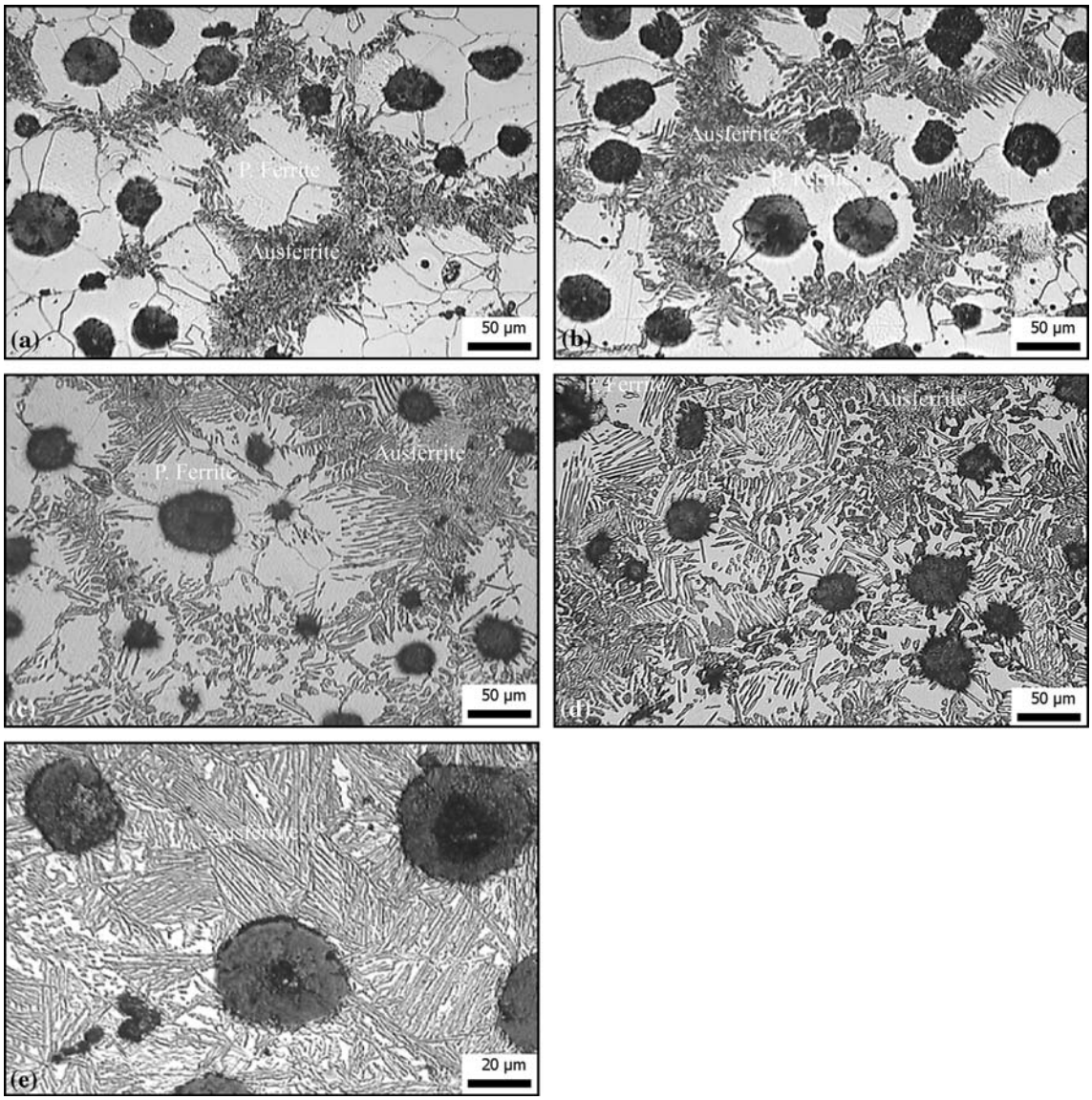

Fig. 3 The microstructures of specimen, (a) 795 (17 AFVF), (b) 805 (26.4 AFVF), (c) 815 (47.2 AFVF), (d) 830 (74 AFVF), and (e) 900 (94.5 AFVF), austempered for 120 min. Etchant: 2% nital. Ausferrite: Bainitic ferrite + High-carbon austenite, P. Ferrite: Proeutectoid ferrite

Similarly, locally deformed ferrite between graphite cavities, having cracked and separated, is shown in Fig. 5(b, arrow b). Locally deformed high-carbon austenite particles, having cracked and also separated, is shown in Fig. 5(c, arrow a).

The decohesion type of voids were more frequent in the necked region. In the vicinity of the graphite nodules, the wider areas of the ferrite phase are deformed considerably as Fig. 5(b) indicates. Considerable elongation of cavities is observed in the specimen with low AFVFs, reflecting the higher deformability (Fig. 5b, arrow a).

On the other hand, in the specimens [830 (75 AFVF) and 815 (47.2 AFVF)], the ausferrite structure surrounding graphites in ferrite-ausferrite matrix with high AFVF (Fig. 5d, e) seems to restrict the stretching of graphite cavity, confirming the low ductility of this material.

As expected, the microvoid density increased near the fracture surface. High density of microvoids near the fracture surface is generally associated with high true strain in this region. During tensile testing, failure of ADI has been attributed to void formation, which has been observed primarily within the necked region at high local strain (Ref 4, 24, 28-35).

Comparing between Fig. 5(b) and (e), the clearances between the graphite nodules could be seen and their corresponding cavities are observed to be larger in specimen 795 (17 AFVF) with low AFVF than specimen 830 (75 AFVF) with high AFVF. This is believed to be due to larger plastic deformation of ferrite around graphite nodules in specimen 795 (17 AFVF) than in 830 (75 AFVF) or 815 (47.2 AFVF). The degree of continuity of ausferritic structure network along the intercellular boundary could be an important factor in determining ferrite deformation degree around graphite nodules.

As mentioned before, in this study, austempering from different ICATs produced ausferritic structures with different AFVFs restricted to eutectic cell boundaries and an isolated, quasi-continuous or continuous network of ausferritic structure along the intercellular boundary depending on AFVF (Fig. 3a-d). In the specimen with higher AFVF, ferrite around the graphite nodules is completely surrounded by ausferritic structure as

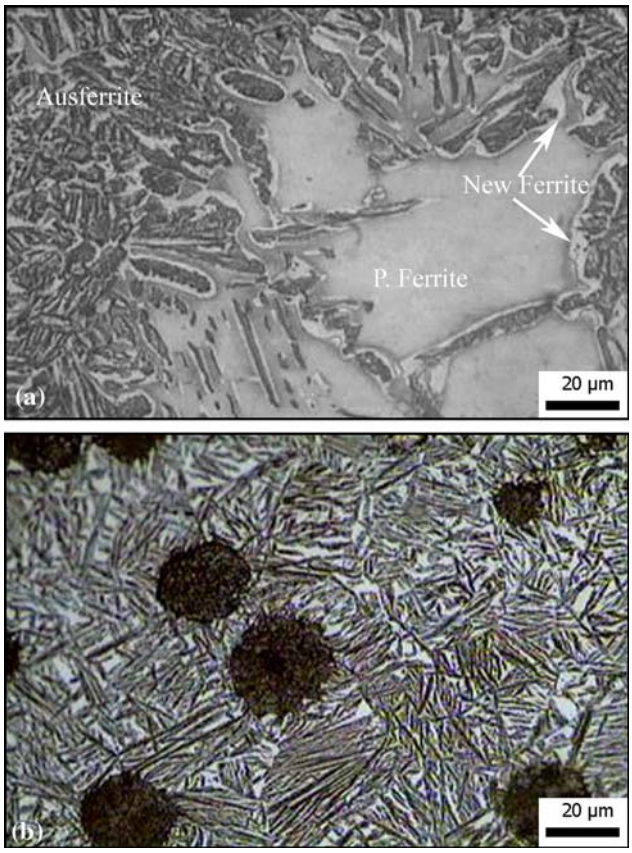

Fig. 4 Microstructures of specimens, (a) 815(47.2 AFVF) and (b) 900(94.5 AFVF), austempered for 120 min. Etchant: 2% nital + Boiling chromate. Ausferrite: Bainitic ferrite + High-carbon austenite, P. Ferrite: Proeutectoid ferrite

shown in Fig. 3(d) and (e). In such a microstructure, high-strength ausferritic structure restricts deformation of ferrite under tensile loading. This can be understood from the necked micrograph of specimen 830 (75 AFVF) or 815 (47.2 AFVF) in Fig. 3(d) and (e) in which graphite nodule keeps its original sphere shape in the direction of straining. This indicates that ferrite around the graphite did not deform to sufficient extent to turn graphite shape into oval as graphite in the fully ferrite matrix (Fig. 5a) or in the matrix with low AFVF (Fig. 5b). This result confirms that the ductility decreased with increasing continuity of ausferritic structure along the intercellular boundaries.

In the case of conventionally heat-treated samples with fully ausferritic structure throughout the specimen generally, microvoids nucleated at the interface between the graphite nodules and the surrounding matrix (Fig. 5f, arrow a) and at high-carbon austenite particles. Nucleation of voids at high-carbon austenite particles starts either by decohesion at the ferrite-high carbon austenite interface (Fig. 5f, arrow b) or brittle fracture of the high-carbon austenite particles (Fig. 5f, arrow c).

It is to be pointed out that little deformation with no stretching around the graphite nodules occurred in this sample as shown in Fig. 5(g). The ausferrite structure surrounding graphites in the ferrite-ausferrite matrix with high AFVF seems to restrict the stretching of graphite cavity. This structure indicates the lack of plastic deformation occurring in the matrix. In comparison with the results obtained for fully ferritic matrix and ADI with DMS, it was noticed that the clearances between the graphite nodules and their corresponding cavities are observed to be tighter as indicated by arrows in Fig. 5(g, arrow a) when compared with Fig. 5(b, arrow a). This very small clearance indicates slight occurrence of plastic deformation around the graphite nodules.

3.2.2 Fractography. The fracture surface of specimen having a fully ferrite matrix is shown in Fig. 6(a). The notable feature of fracture in this figure is the debonding of graphite nodules from the surrounding ferrite structure and a dimple pattern of fracture. The dimple depressions in the fracture surface are evidence of ductile fracture (Fig. 6a). The features shown in this figure suggest that ferrite deforms to a great extent before the onset of fracture, which starts by the formation and coalescence of voids. Microvoid coalescence seems to be the dominant form of fracture. This figure also shows the relatively larger cavity size in comparison with the graphite nodule size. Formation of cavity may be attributed to decohesion at the graphite and surrounding ferrite matrix. The dimple pattern around the graphite nodules shows the deformation of the surrounding ferrite matrix during the final period of straining up to fracture.

In the fracture surface micrographs of ADI with DMS and low AFVFs [795 (17 AFVF) and 805 (26.4 AFVF)], the notable features are: decohesion at graphite nodule and surrounding ferrite, large and shallow dimples in the ausferritic areas, and deep equiaxed dimples in the ferritic areas (Fig. 6b, c). In these figures, cavity size in comparison with the graphite nodule is a good indication of deformability of ADI with different AFVFs.

As shown in Fig. 6(b) to (e), the clearances between the graphite nodules and their corresponding cavities changes from larger to tighter with increasing AFVF. The small clearance indicates slight occurrence of plastic deformation around the graphite nodules. As mentioned before, the links between ausferritic structures along the intercellular boundaries in the matrix increases with increasing AFVF (Fig. 3a-d).

In the fracture surface of specimen 830 having the highest AFVF of 75% among the DMS, the dominant form of fracture surface was a quasi-cleavage type (Fig. 6e). On the other hand, the specimen with 47.2% showed mostly ductile dimples (Fig. 6d) with a quasi-cleavage facet.

In the DMS specimen with low AFVFs, cleavage facets were not observed (Fig. 6b, c). This suggests that the critical stress for cleavage had not been achieved in the austenite at the moment of final fracture. Possibly this is due to the low carbon content of austenite in these samples for the same austempering time, since control over the ICAT can play an important role in controlling the austenite volume fraction (AFV) and its carbon content. In the case of iron with ~3.5% carbon content, the AVF and its carbon content decreases with decreasing ICAT as predicted by the lever rule (Ref 12).

Figure 6(f) shows the fracture surface of conventionally heat-treated samples with fully ausferritic structure. The fracture modes revealed slight plastic deformation around the graphite nodules, and fracture mechanism are a mixture of quasi-cleavage and a dimple pattern, reflecting the moderate ductile nature of the ausferritic structure.

In comparison with the results obtained for fully ferritic matrix and ADI with DMS, it was noticed that the clearances between the graphite nodules and their corresponding cavities are observed to be tighter as indicated by arrows in Fig. 6(f) when compared with Fig. 6(a). This small clearance indicates

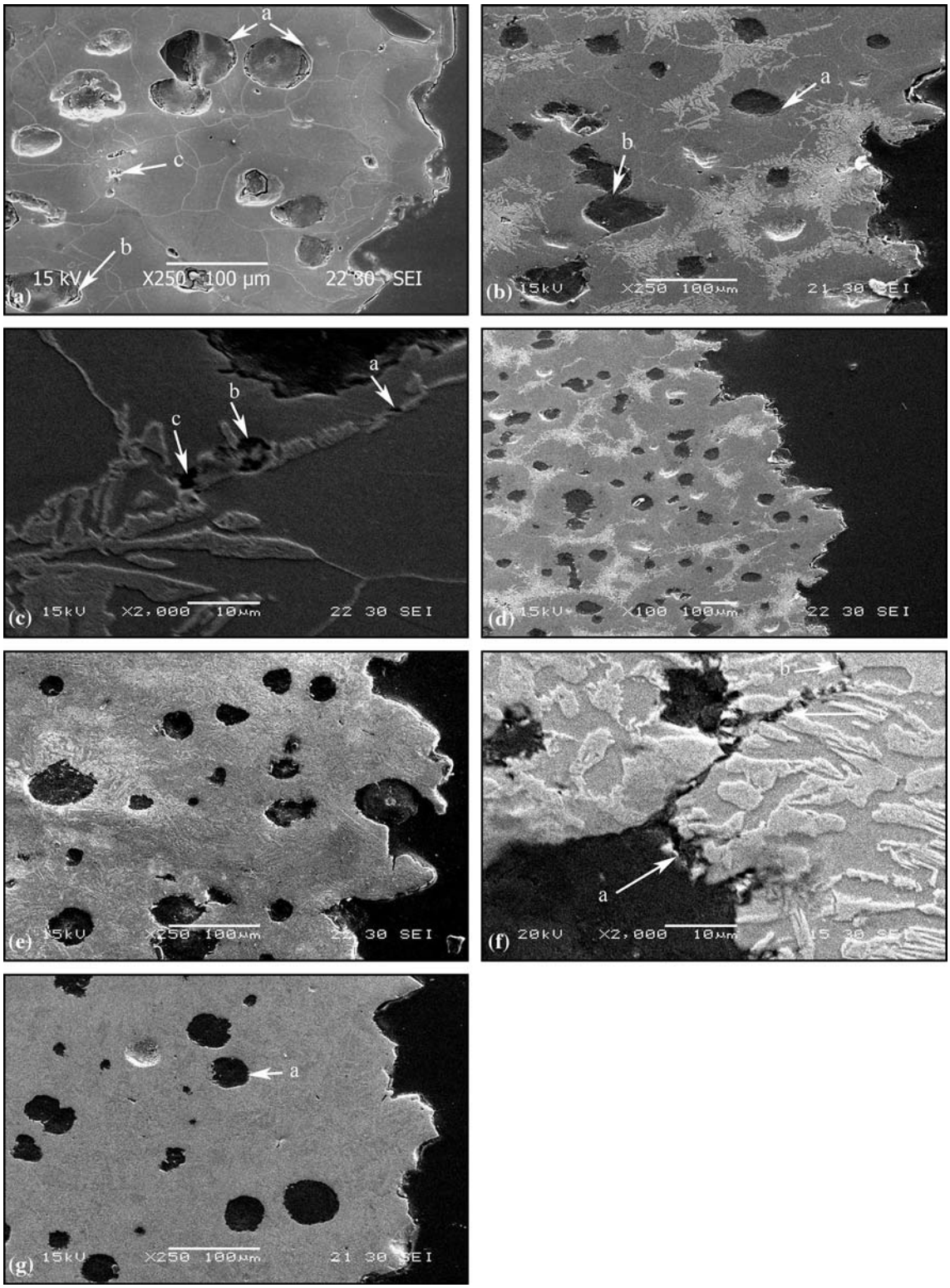

Fig. 5 Matrix deformation and microvoid formation near the fracture surface for specimens (a) as cast, (b) 795(17 AFVF), (c) 805(26.4 AFVF), (d) 815(47.2 AFVF), (e) 830(74 AFVF), and (f, g) 900(94.5 AFVF)

slight occurrence of plastic deformation around the graphite nodules.

The different features of the fracture surfaces show that ferrite volume fraction or AFVF play an important role to determine fracture mode, since ferrite fails in a more ductile fashion and its contribution to the fracture resistance increases with increasing ferrite volume fraction. In the specimen with a higher AFVF or low ferrite volume fraction, the majority of the fracture surface shows a quasi-cleavage pattern of fracture, reflecting the low ductility and fracture energy of this material

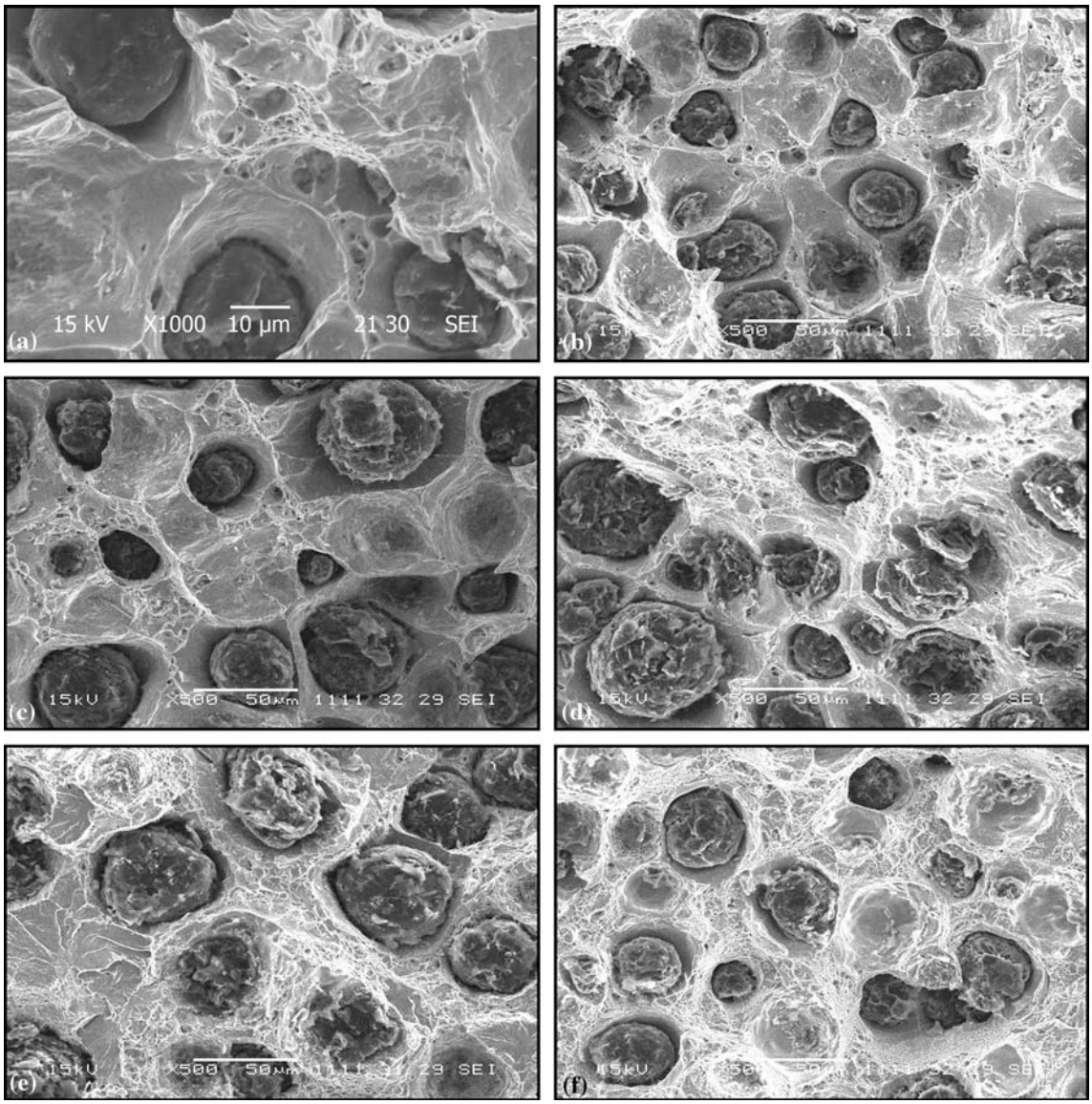

Fig. 6 The fracture surfaces for specimens (a) as cast, (b) 795(17 AFVF), (c) 805(26.4 AFVF), (d) 815(47.2 AFVF), (e) 830(74 AFVF), and (f) 900(94.5 AFVF)

(Fig. 6f) compared with those specimens with low AFVF (Fig. 6b, c).

In the current study, the relationship between the fractographic studies and the tensile properties indicates that generally the cracks are initiated at the interface between the graphite nodules and the surrounding structure. Thus, introducing a moderate higher-strength ausferritic structure into ferrite matrix requires a higher strength to initiate a crack and this strength increases with increasing AFVF. In this case, the low-strength ferrite in the rest of the matrix will be plastically deformed. It is reasonable to accept that the moderate strength of the ausferrite structure affected the strength of the material by means of delaying the crack initiation. However, the more ductile nature of the ferrite-ausferrite structure and its ability to deform plastically, compared with the fully ausferritic structure, did not considerably restrain the plastic flow of the ferrite phase. Thus, the failure occurred in a ductile fashion and the material does not lose much of its ductility.

Further contribution to higher ductility in ADI with DMS may come from new ferrite due to its higher deformability (Ref 12, 13). As mentioned before, the new ferrite only exists in ADI with DMS (Table 2).

4. Conclusions

1. The fracture modes of conventional ADI revealed slight plastic deformation around the graphite nodules, and the matrix failed in a brittle manner as evidenced by a mixture of quasi-cleavage and a dimple pattern reflecting the moderate ductile nature of the ausferritic structure. However, the fracture mode of specimen having a fully ferritic matrix is ductile as evidenced by the presence of ripple and dimple patterns.

2. In determining fracture behavior of ADI with different ausferrite volume fractions, the different fracture mechanism corresponds to the different level of ausferrite volume fractions and the continuity of ausferritic structure along the intercellular boundaries. The continuity of ausferritic structure increases with increasing ausferrite volume fractions and the fracture pattern changes from ductile to brittle.

Acknowledgments

The authors wish to acknowledge the financial supports of Gazi University Scientific Research Fund (Project code 07/2007-30 and 07/2005-25). The authors also indebted to ALFA Casting Company Ankara, Turkey for castings and to Saraykoy Nuclear Research and Education Center (TAEK-SANAEM) for providing x-ray facilities. Our acknowledgements are also extended to the UMIST Manchester Materials Science Centre for the provision of its laboratory facilities and to its staff who have assisted us throughout our study.

References

1. R.C. Voigt, L.M. Eldoky, and H.S. Chiou, Fracture of Ductile Cast Irons with Dual Matrix Structure, *AFS Trans.*, 1986, **94**, p 645–656 (in English)
2. A.M. Rashidi and M. Moshrefi-Torbati, Effect of Tempering Conditions on the Mechanical Properties of Ductile Cast Iron with Dual Matrix Structure (DMS), *Mater. Lett.*, 2000, **45**(3–4), p 203–207 (in English)
3. J. Aranzabal, G. Serramoglia, and D. Rousiere, Development of a New Mixed (Ferritic-Ausferritic) Ductile Iron for Automotive Suspension Parts, *Int. J. Cast Met. Res.*, 2003, **16**(1–3), p 185–190 (in English)
4. T. Kobayashi and H. Yamamoto, Development of High Toughness in Austempered Type Ductile Cast Iron and Evaluation of its Properties, *Metall. Mater. Trans. A*, 1988, **19**(2), p 319–327 (in English)
5. T. Kobayashi and S. Yamada, Effect of Holding Time in the ($\alpha + \gamma$) Temperature Range on Toughness of Specially Austempered Ductile Iron, *Metall. Mater. Trans. A*, 1996, **27**(7), p 1961–1971 (in English)
6. Z.R. He, G.X. Lin, and S. Ji, Deformation and Fracture Behaviour of Cast Iron with Optimized Microstructure, *Mater. Charact.*, 1997, **38**(4–5), p 251–258 (in English)
7. M. Hafiz, Tensile Properties and Fracture of Ferritic SG-Iron Having Different-shell Structure, *Z. Metallkd.*, 2001, **92**(11), p 1258–1261 (in English)
8. R. Kazerooni, A. Nazarboland, and R. Elliot, Use of Austenitising Temperature in Control of Austempering of an Mn-Mo-Cu Alloyed Ductile Iron, *Mater. Sci. Technol.*, 1997, **13**(12), p 1007–1015 (in English)
9. M. Cerah, K. Kocatepe, and M. Erdogan, Influence of Martensite Volume Fraction and Tempering Time on Tensile Properties of Partially Austenitized in the ($\alpha + \gamma$) Temperature Range and Quenched + Tempered Ferritic Ductile Iron, *J. Mater. Sci.*, 2005, **40**(13), p 3453–3459 (in English)
10. M. Erdogan, K. Kocatepe, and M. Cerah, Influence of Intercritical Austenitising and Tempering Time and Martensite Volume Fractions on Tensile Properties of Ferritic Ductile Iron with Dual Matrix Structure, *Int. J. Cast Met. Res.*, 2006, **19**(4), p 248–253 (in English)
11. K. Kocatepe, M. Cerah, and M. Erdogan, The Tensile Fracture Behaviour of Intercritically Annealed and Quenched + Tempered Ferritic Ductile Iron with Dual Matrix Structure, *Mater. Des.*, 2006, **28**(1), p 172–181 (in English)
12. M. Erdogan, V. Kilicli, and B. Demir, Transformation Characteristics of Ductile Iron Austempered from Intercritical Austenitizing Temperature Ranges, *J. Mater. Sci.*, 2009, **44**(5), p 1394–1403 (in English). doi:10.1007/s10853-006-1415-7
13. V. Kilicli and M. Erdogan, Tensile Properties of Partially Austenitized and Austempered Ductile Irons with Dual Matrix Structures, *Mater. Sci. Technol.*, 2006, **22**(8), p 919–928 (in English)
14. B.D. Cullity, *Elements of X-Ray Diffraction*, 2nd ed., Addison-Wesley, Reading, MA, 1978, p 411–412
15. C. Labrecque and M. Gagne, Ductile Iron: Fifty Years of Continuous Development, *Can. Met. Q.*, 1998, **37**(5), p 343–378 (in English)
16. A. Trudel and M. Gagne, Effect of Composition and Heat Treatment Parameters on the Characteristics of Austempered Ductile Irons, *Can. Met. Q.*, 1997, **36**(5), p 289–298 (in English)
17. N. Darwish and R. Elliot, Austempering of Low Manganese Ductile Irons. 1. Processing Window, *Mater. Sci. Technol.*, 1993, **9**(7), p 572–585 (in English)
18. S. Yazdani and R. Elliot, Influence of Molybdenum on Austempering Behaviour of Ductile Iron. Part 1. Austempering Kinetics and Mechanical Properties of Ductile Iron Containing 0-13%Mo, *Mater. Sci. Technol.*, 1999, **15**(5), p 531–540 (in English)
19. W. Zhao and G. Wang, The Control of the Chemical Composition, Microstructure and Mechanical Properties of Beinite Ductile Iron for Liner Plates, *J. Mater. Process. Technol.*, 1999, **95**(1–3), p 27–29 (in English)
20. M. Bahmani, R. Elliot, and N. Varahram, The Austempering Kinetics and Mechanical Properties of an Austempered Cu-Ni-Mo-Mn Alloyed Ductile Iron, *J. Mater. Sci.*, 1997, **32**(18), p 4783–4791 (in English)
21. J. Mallia, M. Grech, and R.E. Smallman, Effect of Silicon Content on Transformation Kinetics of Austempered Ductile Iron, *Mater. Sci. Technol.*, 1998, **14**(5), p 452–460 (in English)
22. S.K. Putatunda, Influence of Austempering Temperature on Fracture Toughness of a Low Manganese Austempered Ductile Iron (ADI), *Mater. Manuf. Process.*, 2001, **16**(2), p 245–263 (in English)
23. H. Bayati, R. Elliot, and G.W. Lorimer, Influence of Austenitising Temperature on Austempering Kinetics of High Manganese Alloyed Ductile Cast-Iron, *Mater. Sci. Technol.*, 1995, **11**(8), p 776–786 (in English)
24. J. Aranzabal, I. Gutierrez, and J.J. Urcola, Influence of Heat-Treatments on Microstructure of Austempered Ductile Iron, *Mater. Sci. Technol.*, 1994, **10**(8), p 728–737 (in English)
25. M. Baydogan and H. Çimenoglu, The Effect of Austempering Time on Mechanical Properties of a Ductile Iron, *Scand. J. Met.*, 2001, **30**(6), p 391–395 (in English)
26. C.R.F. Azevedo, A.A. Garboggini, and A.P. Tschipitschin, Effect of Austenite Grain-Refinement on Morphology of Product of Bainitic Reaction in Austempered Ductile Iron, *Mater. Sci. Technol.*, 1993, **9**(8), p 705–710 (in English)
27. R.D. Lawson, D.K. Matlock, and G. Krauss, Etching Technique for Microalloyed Dual-Phase Steels, *Metallography*, 1980, **13**(1), p 71–87 (in English)
28. A. Refaey and N. Fatahalla, Effect of Microstructure on Properties of ADI and Low Alloyed Ductile Iron, *J. Mater. Sci.*, 2003, **38**(2), p 351–362 (in English)
29. P.Q. Dai, Z.R. He, W.Q. Wu, and Z.Y. Mao, Mechanical Behaviour of Graphite in Fracture of Austempered Ductile Iron, *Mater. Sci. Technol.*, 2002, **18**(9), p 1052–1056 (in English)
30. M. Hafiz, Mechanical Properties of SG-Iron Subjected to Variable and Isothermal Austempering Temperatures Heat Treatment, *Mater. Sci. Eng. A*, 2003, **340**(1–2), p 1–7 (in English)
31. B. Bosnjak, B. Radulovic, K.P. Tonev, and V. Asanvic, Microstructural and Mechanical Characteristics of Low Alloyed Ni-Mo-Cu Austempered Ductile Iron, *ISIJ Int.*, 2000, **40**(12), p 1246–1252 (in English)
32. M. Hafiz, Mechanical Properties of SG-Iron with Different Matrix Structure, *J. Mater. Sci.*, 2001, **36**(5), p 1293–1300 (in English)
33. D.C. Wen and T.S. Lei, The Mechanical Properties of a Low Alloyed Austempered Ductile Iron in the Upper Ausferrite Region, *ISIJ Int.*, 1999, **39**(5), p 493–500 (in English)
34. L. Sidjanin, R.E. Smallman, and S.M. Boutorabi, Microstructure and Fracture of Aluminum Austempered Ductile Iron Investigated Using Electron-Microscopy, *Mater. Sci. Technol.*, 1994, **10**(8), p 711–720 (in English)
35. S.K. Putatunda and P.K. Gadicherla, Influence of Austenitizing Temperature on Fracture Toughness of a Low Manganese Austempered Ductile Iron (ADI) with Ferritic as Cast Structure, *Mater. Sci. Eng. A*, 1999, **268**(1–2), p 15–31 (in English)